Discovery of drugs to treat cytokine storm-induced cardiac dysfunction using human cardiac organoids

Richard J Mills[1], Sean J Humphrey[2], Patrick RJ Fortuna[1], Gregory A Quaife-Ryan[1], Neda R Mehdiabadi[3], Lynn Devilée[1], Holly K Voges[1], Liam T Reynolds[1], Sophie Krumeich[1], Ellen Mathieson[1], Brendan Griffen[4], Drew Titmarsh[4], Enzo R Porrello[3,5], Mark J Smyth[1], Christian R Engwerda[1], Kelli PA MacDonald[1], Tobias Bald[1], David E James[2,6], James E Hudson[1,*]

[1]QIMR Berghofer Medical Research Institute, Brisbane 4006, QLD, Australia

[2] Charles Perkins Centre, School of Life and Environmental Science, The University of Sydney, Sydney 2006, NSW, Australia

[3]Murdoch Children's Research Institute, The Royal Children's Hospital, Melbourne 3052, VIC, Australia

[4]Dynomics Inc., San Mateo, CA 94401, United States of America and Dynomics Pty Ltd, Brisbane, QLD 4000, Australia

[5]Department of Physiology, School of Biomedical Sciences, The University of Melbourne, Melbourne 3052, VIC, Australia

[6]Faculty of Medicine and Health, The University of Sydney, Sydney, NSW 2006, Australia

* Corresponding author

Please address correspondence to:

Associate Professor James E. Hudson

QIMR Berghofer Medical Research Institute

Herston, Brisbane

QLD, 4006, Australia

Tel: +61 7 3362 0141

Email: james.hudson@qimrberghofer.edu.au

SUMMARY

SARS-CoV2 infection leads to cardiac injury and dysfunction in 20-30% of hospitalized patients[1] and higher rates of mortality in patients with pre-existing cardiovascular disease[2,3]. Inflammatory factors released as part of the 'cytokine storm' are thought to play a critical role in cardiac dysfunction in severe COVID-19 patients[4]. Here we use human cardiac organoids combined with high sensitivity phosphoproteomics and single nuclei RNA sequencing to identify inflammatory targets inducing cardiac dysfunction. This state-of-the-art pipeline allowed rapid deconvolution of mechanisms and identification of putative therapeutics. We identify a novel interferon-γ driven BRD4 (bromodomain protein 4)-fibrosis/iNOS axis as a key intracellular mediator of inflammation-induced cardiac dysfunction. This axis is therapeutically targetable using BRD4 inhibitors, which promoted full recovery of function in human cardiac organoids and prevented severe inflammation and death in a cytokine-storm mouse model. The BRD inhibitor INCB054329 was the most efficacious, and is a prime candidate for drug repurposing to attenuate cardiac dysfunction and improve COVID-19 mortality in humans.

MAIN

The range of cardiac sequelae reported in patients with COVID-19, include acute coronary syndromes, cardiomyopathy, acute pulmonary heart disease, arrhythmias and heart failure[5]. There have been multiple proposed aetiologies for these, yet clear mechanistic insight is lacking[5]. There is a severe inflammatory response in 5% of COVID-19 patients, associated with septic shock[2]. This leads to a drop in blood pressure, and approximately 30% of hospitalized patients with COVID-19 require vasopressors to improve blood pressure[6]. Furthermore, 68-78% have sustained cardiac dysfunction[7,8]. In severe infections, inflammation associated with a 'cytokine storm' can directly cause cardiac dysfunction and pathology. For example, TNF is a well-known inflammatory effector associated with heart failure that causes systolic dysfunction[9]. Inflammation-induced cardiac dysfunction could have broad consequences and lead to inadequate organ perfusion and immune cell infiltration, further exacerbating disease. Thus, preventing cytokine-induced cardiac dysfunction may limit severe outcomes in COVID-19 patients. However, targeted treatment strategies, particularly in severe infections such as COVID-19, are currently lacking.

Several anti-inflammatory agents have shown clinical benefit for the acute management of COVID-19. Dexamethasone improved 28-day mortality in COVID-19 patients receiving invasive mechanical ventilation or oxygen at randomization[10]. Additionally, Janus kinase (JAK)/signal transducer and activator of transcription (STAT) (ruxolitinib and baricitinib) and IL-6R inhibitors (tocilizumab and sarilumab) are currently in COVID-19 clinical trials. However, a limitation of systemic immunosuppression is that it may impede viral clearance thus potentially exacerbating disease[11]. To circumvent this, we aimed to identify cardiac-specific inflammatory targets that trigger cardiac dysfunction in response to the cytokine storm, reasoning that these might provide a much-needed safer therapeutic option.

Here, we utilize multi-cellular human pluripotent stem cell-derived cardiac organoids (hCO) combined with phosphoproteomics and single nuclei RNA-sequencing to identify therapeutic targets and treatments for cardiac dysfunction. We recently adapted our hCO system[12,13] to include co-culture with endothelial cells, that form enhanced branched endothelial structures surrounded by pericytes (**Extended Data Fig. 1**), together with an optimized culture environment that reflects a maturation stage; mimicking the postnatal metabolic environment[13] followed by reversion to a more adult metabolic substrate provision (see **Methods**). This platform enabled

rapid screening of cytokine combinations that mimic the COVID-19-induced 'cytokine storm' and cardiac dysfunction, with subsequent application of omic assays and drug screening'[11].

Cytokine-induced cardiac dysfunction

We began by examining the effects of a range of pro-inflammatory cytokines on cardiac function in our hCO[11,14]. Inflammatory molecules tested were TNF, IL-1β, IFN-γ, IL-6, IL-17A, and G-CSF, as well as pathogen-associated molecular patterns including poly(I:C) to mimic dsRNA, and lipopolysaccharide (LPS) to mimic TLR4 activation. Using RNA-seq[13,15], we identified that the expression of the following receptors *IL1R1*, *TNFRSF1A*, *TNFRSF1B*, *IFIH1*, *MYH88*, *IL6ST*, *IFNAR1*, *IL6R*, *TMEM173*, *IL17RA*, *IL17RB*, *IL17RC*, *IL17RD*, *IL17RE*, *IFNGR1*, *TLR3*, and *TLR4* were at similar or higher levels in our hCO compared to adult human heart (**Extended Data Fig. 2a**). In adult mouse hearts many of these are enriched in non-myocyte populations[16] (**Extended Data Fig. 2b**). We used single nuclei RNA sequencing (snRNA-seq) to assess cell specificity in our enhanced hCO (Voges et al., In Revision). Mapping to human heart snRNA-seq[17] revealed the presence of pro-epicardial/epicardial cells, fibroblasts, activated fibroblasts/pericytes and cardiomyocytes (**Extended Data Fig. 2c,d**). Some cardiomyocytes were fetal-like, however there was a distinct sub-cluster that mapped adjacent to adult ventricular cardiomyocytes from human hearts[18] (**Extended Data Fig. 2e**). The cytokine/pro-inflammatory receptors were expressed across different cell types, but were enriched and more highly expressed in epicardial cells and fibroblasts (**Extended Data Fig. 2f**)[13,15]. We screened inflammatory factors in all pair-wise combinations in hCOs with multiple functional measurements including contractile force, rate, activation kinetics and relaxation kinetics[12,13] (**Fig. 1a**). TNF caused a reduction in force, while IFN-γ, IL-1β, poly(I:C) and LPS caused diastolic dysfunction characterized by a preserved contractile force but prolonged time from peak to 50% relaxation (**Extended Data Fig. 3**). A secondary full-factorial screen of TNF, IFN-γ, IL-1β, and poly(I:C), once again revealed that TNF induced systolic dysfunction (**Fig. 1b,d**) with an EC_{50} of 1 ng/mL at 48 hours (**Extended Data Fig. 4a**). A combination of IFN-γ, IL-1β and poly(I:C) induced diastolic dysfunction (**Fig. 1c,e**), however also decreased the beating rate which may influence the kinetics of contraction (**Extended Data Fig. 5, Supplementary Video 1,2**). Changes in rate were not responsible for increased relaxation time, as hCO paced at 1 Hz retained the severe diastolic dysfunction phenotype (**Fig. 1f, Supplementary Video 3,4**). Individually, IFN-γ and IL-1β caused concentration-dependent diastolic dysfunction with a low EC_{50} of 0.8 ng/mL at 48 hours and 3 ng/mL at 24 hours, respectively, while poly(I:C) was not able to induce dysfunction alone (**Extended Data Fig. 4b-d**). These results were confirmed in an independent cell line and overall the combination of IFN-γ, IL-1β and poly(I:C) induced the most consistent, robust diastolic dysfunction (**Extended Data Fig. 6a-e**). Taken together this demonstrates that TNF induces systolic dysfunction consistent with previous *in vitro*[19] and *in vivo*[20] studies and a combination of IFN-γ, IL-1β and poly(I:C) induces severe diastolic dysfunction in hCO. The dominant factor identified causing diastolic dysfunction, IFN-γ (**Extended Data Fig. 6c**), is generally elevated in heart failure patients, but its role in heart failure is contradictory in animal models with both detrimental and beneficial effects reported[21].

Mechanisms driving cardiac cytokine storm-induced dysfunction

The most common cardiac dysfunction in hospitalized COVID-19 patients is right ventricular dysfunction or left ventricular diastolic dysfunction[7]. Therefore, we chose to interrogate the mechanism of diastolic dysfunction induced by IFN-γ, IL-1β and poly(I:C), from here on referred

to as 'cardiac cytokine storm' (CS). Since protein phosphorylation is intimately linked with all biological functions[22] we reasoned that measuring the global phosphoproteome in hCO would provide an accurate fingerprint of the mechanistic targets of the 'cardiac cytokine storm'. Employing the latest developments of our phosphoproteomics technology[23,24], enabled identification of over 7,000 phosphosites in each sample, accurately pinpointing 7,927 phosphorylation sites to a single amino acid residue on around 3,000 different phosphoproteins from single-run measurements of 20 organoids yielding < 100 µg of protein each (**Fig. 2a**, **Extended Data Fig. 7**). Preliminary studies using TNF identified several known biological effects of this cytokine including decreased phosphorylation of protein kinase A and increased phosphorylation of ADRK1 (also known as GRK2), supporting our approach. Applying this technology to the cardiac cytokine storm treatment revealed 91 phosphosites that were consistently elevated across three biological replicates (**Fig. 2b**). These sites were enriched for terms relating to proliferation, with transcription factors over-represented with 35 sites found on transcription factors or chromatin-binding proteins and 13 associated with the biological process term 'cell proliferation' (FDR < 0.05, Fisher exact). Among these was phosphorylation of signal transducer and activator of transcription 1 (STAT1) S727 (median 13.9 fold), as well as two sites on BRD4 (Bromodomain-containing protein 4) S469 and S1083 (median 7.4 and 12.3 fold respectively) (**Fig 2b,c**). In view of the availability of specific small molecule inhibitors for each of these targets or their upstream regulators we focused on these proteins in subsequent functional assays. The cytokine receptor enrichment in non-myocytes (**Extended Data Fig. 2**) and broad expression of key phosphorylation sites such as BRD4 (**Fig. 2b**) suggests a multi-cellular response mediates cardiac dysfunction. We assessed activation of individual cell populations in hCOs using snRNA-seq of ~40 pooled hCOs per condition (**Fig. 3a**) with mapping as described above (CTRL - **Extended Data Fig. 2c,d** and cardiac cytokine storm - **Extended Data Fig.8a,b**). In cytokine storm conditions there was an increase in fibroblast and activated fibroblast number (**Fig. 3b**). Consistently, recently identified markers of fibroblast activation[25] also increased, including *MEOX1*, *SERPINE1* (also known as plasminogen activator inhibitor-1 which induces clotting), *TNC*, *VEGFC*, and *IL4R*, (**Fig. 3c,d**). Fibroblast activation is known to be widely associated with cardiac dysfunction, including in patients with diastolic dysfunction[26].

Prevention of cardiac dysfunction and mortality

We next screened drugs that could potentially prevent cardiac dysfunction under either TNF-induced systolic dysfunction or cardiac cytokine storm-driven diastolic dysfunction (**Fig. 4a**). TNF is known to induce systolic dysfunction via GRK2 mediated repression of β-adrenergic receptor signaling[19]. The selective serotonin reuptake inhibitor, paroxetine hydrochloride, can inhibit GRK2[27], but we found that it was toxic at effective *in vitro* concentrations[28] (**Extended Data Fig. 9a**). GRK2 mediates receptor endocytosis[29], and baricitinib was recently identified as a potential AAK1-mediated endocytosis inhibitor using machine learning[30]. Baricitinib prevented TNF-induced dysfunction in hCO (**Fig. 4b** and **Extended Data Fig. 9a-b**). However, baricitinib was only protective against TNF-induced systolic dysfunction when co-administered with TNF and was not effective after 24 h TNF treatment (**Fig. 4c**), potentially because receptor internalization had already occurred. Additionally, hCO did not recover quickly from TNF-induced systolic dysfunction after the removal of TNF (**Fig. 4c**) indicating that secondary remodeling events may have occurred.

A key signature of diastolic dysfunction under cytokine storm conditions was the increased phosphorylation of transcriptional regulators. STAT1-S727 (**Fig. 2c**) is associated with assembly into chromatin and is required for STAT1 transcriptional and biological activity in response to IFN-γ[31]. The putative STAT1-S727 kinase is CDK8[32], and so we next tested two CDK8 inhibitors SEL120-34A[33] and BI-1347[34] previously shown to reduce STAT1-S727 phosphorylation. We also

tested baricitinib and ruxolitinib two inhibitors of the JAK/STAT pathway. However, none of these compounds, nor a broader spectrum CDK inhibitor flavopiridol, prevented the cardiac cytokine storm-induced diastolic dysfunction (**Extended Data Fig. 10**). Noting flavipiridol was toxic and reduced force and hence all kinetic parameters. Notably, SEL120-34A and BI-1347 specifically attenuated the rate and activation time defects under cardiac cytokine storm conditions (**Extended Data Fig. 10b,c,e,f**), which we validated in additional experiments (**Extended Data 11a-d**) and may still have clinical utility in this setting.

Phosphorylation of the epigenetic regulator BRD4 was increased in cytokine storm treated hCO and we have previously shown that BRD inhibitors reduce relaxation time in immature hCO[12]. BRD inhibitors INCB054329[35], JQ-1[36], and ABBV-744[37] were tested. INCB054329 was capable of preventing cardiac cytokine storm-induced diastolic dysfunction in a dose-dependent manner (**Fig. 4d, Extended Data Fig. 12**) without affecting force or rate (**Extended Data Fig. 10a-g, Supplementary Video 5**). JQ-1 showed improved diastolic function in one hPSC line at the highest concentration (**Extended Data Fig. 10g**), so an additional higher concentration for JQ-1 and ABBV-744 were tested. JQ-1 was capable of protecting hCO against cardiac cytokine storm-induced diastolic dysfunction, although INCB054329 was the most efficacious (**Extended Data 13a,b**). ABBV-744 was not effective, possibly because it is also an inhibitor of the androgen receptor, which causes diastolic dysfunction in human cardiomyocytes[38]. INCB054329 was capable of restoring diastolic function following 24 h of cardiac cytokine storm conditions (**Fig. 4e**). This is potentially because cytokine storm-induced diastolic dysfunction is driven by the presence of the inflammatory mediators, demonstrated by partial hCO recovery 24 h after removing cytokine storm factors (**Fig. 4e**). In patients, all inflammatory factors may be present simultaneously, and we found that INCB054329 could attenuate diastolic dysfunction with all four factors, TNF, IFN-γ, IL-1β, and poly(I:C), present (**Extended Data Fig. 13c**).

Diastolic dysfunction in hCO and human patients with heart failure with preserved ejection fraction (HFpEF) or COVID-19 is associated with fibrosis[26,39] (**Fig. 3**), with BRD4 known to activate extracellular matrix deposition by fibroblasts[40,41]. In addition to this potential mechanism, chronic inflammation caused by obesity, diabetes mellitus, chronic obstructive pulmonary disease, and hypertension cause systemic inflammation which also drives endothelial dysfunction and decreased nitric oxide (NO) availability[42]. This causes iNOS compensation in other cell types, which can cause nitrosylation stress and cardiac dysfunction[43,44]. As BRD4 is broadly expressed in our hCO (**Fig. 4f**), BRD4 inhibition may also protect against these changes. We found cytokine storm decreased *NOS3* mRNA (also known as *eNOS*) and induced *NOS2* mRNA (also known as *iNOS*) ~40 fold in hCO, which in turn could be fully prevented by BRD inhibition without rescue of *eNOS* (**Fig. 4g**).

Finally, we tested the ability of INCB054329 to prevent LPS-induced cytokine storm and lethality *in vivo*. We observed a significant improvement in mortality, where all INCB054329-treated mice survived after 24 h of the LPS-challenge, compared with only 25% in the control group (**Fig. 4h**). Increased survival was associated with significantly reduced levels of the pro-inflammatory cytokines TNF, IL-1β and IFN-γ, which are elevated in COVID-19 patients and drive cardiac dysfunction in hCO (**Fig. 4i, Extended Data Fig. 6a,b**). Furthermore, INCB054329 prevented a fibrotic response and iNOS induction in ventricular myocardium (**Extended Data Fig. 14a,b**). Taken together, INCB054329 has potent and robust effects on improvement of cardiac function and prevention of mortality due to a cytokine storm.

DISCUSSION

In this study we show that inflammatory mediators directly impact cardiac function in hCO, a model free from the secondary effects and neurohormonal compensation present *in vivo*. We find that a combination of classical viral response cytokines IFN-γ and IL-1β, combined with dsRNA – "cardiac cytokine storm" - cause severe diastolic dysfunction with 20-50% increases in relaxation time without decline in systolic function. This is consistent with clinical data from HFpEF patients, where cardiomyocytes have increased time to 50% relaxation time by ~13-18% (with similar overall values of 100-150 ms in both humans and hCO)[45]. A reason why cardiovascular risk factors for HFpEF are also risk factors for mortality in COVID-19 patients, may be that the underlying chronic inflammation and cardiac dysfunction becomes further exacerbated by the acute, inflammatory response in patients with COVID-19. Prolonged relaxation also increases the risk of arrhythmias, which have been widely reported in COVID-19 patients[46]. Arrhythmic events increased in cardiac cytokine storm conditions across our 6 experiments, for which INCB054329 also conferred protection (**Extended Data Fig. 15a-c**).

We identify a therapeutically targetable IFNγ-BRD4 -fibrosis/iNOS axis as a key intracellular mediator of inflammation-induced cardiac dysfunction, which functions independently of JAK/STAT. BRD4 inhibition reduced inflammatory cytokine production, fibroblast activation, and compensatory iNOS production, all of which drive cardiac dysfunction. Previously, the BRD inhibitor GSK525762A has shown efficacy in mouse cytokine storm models[47] and JQ-1 has shown efficacy in small animal cardiac injury models[48]. However, in our studies INCB054329 was far more potent than JQ-1, and ABBV-744 had no efficacy in improving cardiac cytokine storm induced dysfunction. This indicates that BRD inhibitors need to be carefully selected for cardiac efficacy, despite their broad utility for a variety of clinical conditions[49]. Taken together, the efficacy and known safety profile of INCB054329 (NCT02431260)[50] make it a prime candidate for drug repurposing to attenuate cardiac dysfunction and improve COVID-19 mortality in humans.

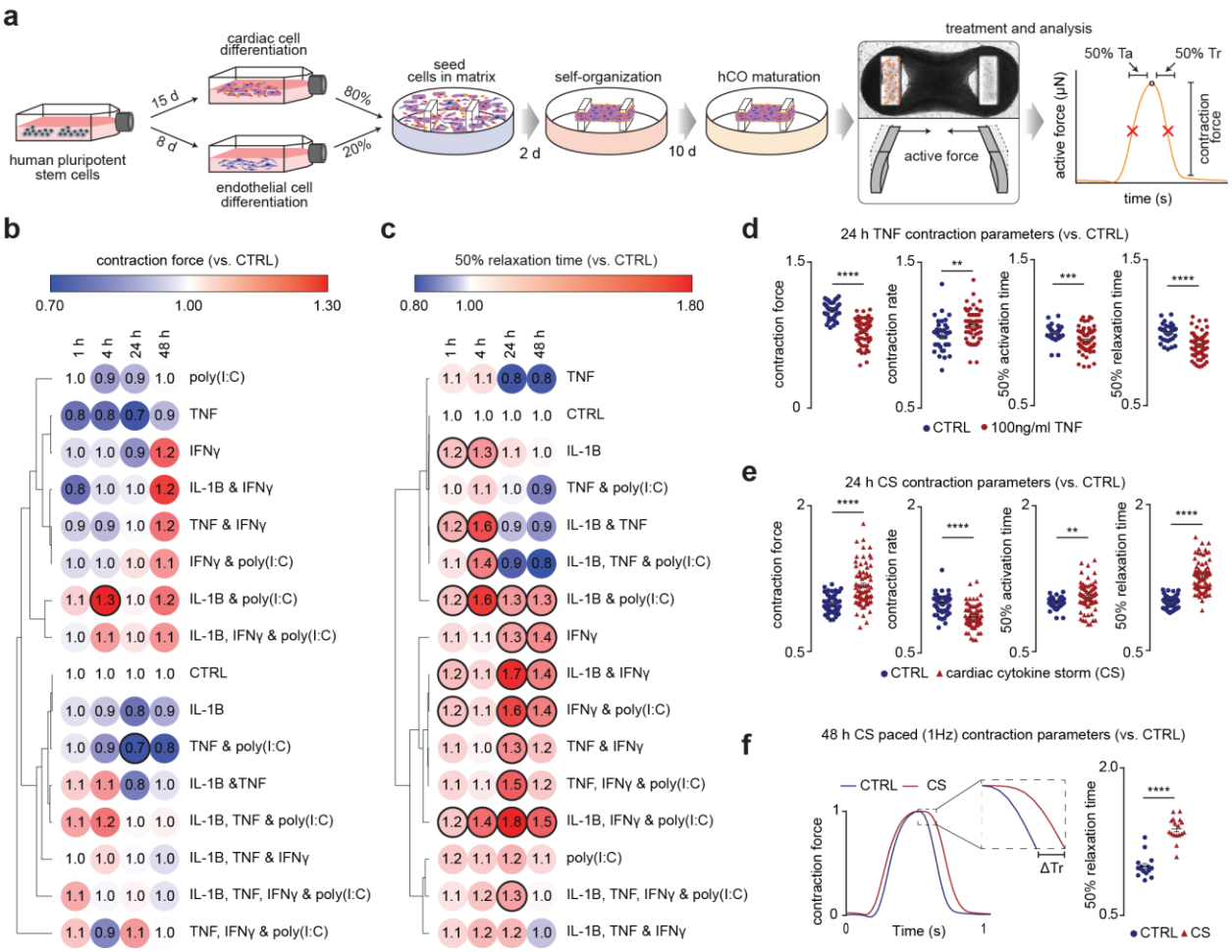

Figure 1: Identification of pro-inflammatory factors driving cardiac dysfunction.

a) Schematic of experimental pipeline.
b) Impact of inflammatory modulators on force (systolic function). Bold outline indicates p <0.05 using a one-way ANOVA with Dunnett's multiple comparisons test comparing each condition to CTRL at its' time point. n= 3-5 hCOs per condition from 1 experiment. hPSC cardiac cells- AA, Endothelial cells- RM3.5.
c) Impact of inflammatory modulators on time to 50% relaxation (diastolic function). Bold outline indicates p <0.05 using a one-way ANOVA with Dunnett's multiple comparisons test comparing each condition to CTRL at its' time point. n= 3-5 hCOs per condition from 1 experiment. hPSC cardiac cells- AA, Endothelial cells- RM3.5.
d) TNF causes systolic dysfunction. n = 37 and 63 hCOs for CTRL and TNF conditions, respectively from 6 experiments. hPSC cardiac cells- HES3, Endothelial cells- RM3.5 or CC. ** p<0.01, *** p<0.001, **** p<0.0001, using Student's t-test.
e) Cytokine storm causes diastolic dysfunction n = 49 and 73 hCOs for CTRL and cardiac cytokine storm conditions, respectively from 6 experiments. hPSC cardiac cells- HES3, Endothelial cells- RM3.5 or CC. ** p<0.01, **** p<0.0001, using Student's t-test.
f) Representative force curve of hCO under control (CTRL) and cardiac cytokine storm (CS) conditions (1 Hz) 48 h after treatment. Relaxation of CTRL and CS under paced conditions (1 Hz) 48 h after treatment. n = 15 and 17 hCOs per condition, respectively, from 3

experiments. hPSC cardiac cells- HES3, Endothelial cells- RM3.5 or CC. **** $p<0.0001$, using Student's t-test.

CS – cardiac cytokine storm, Ta – time from 50% activation to peak, Tr – time from peak to 50% relaxation

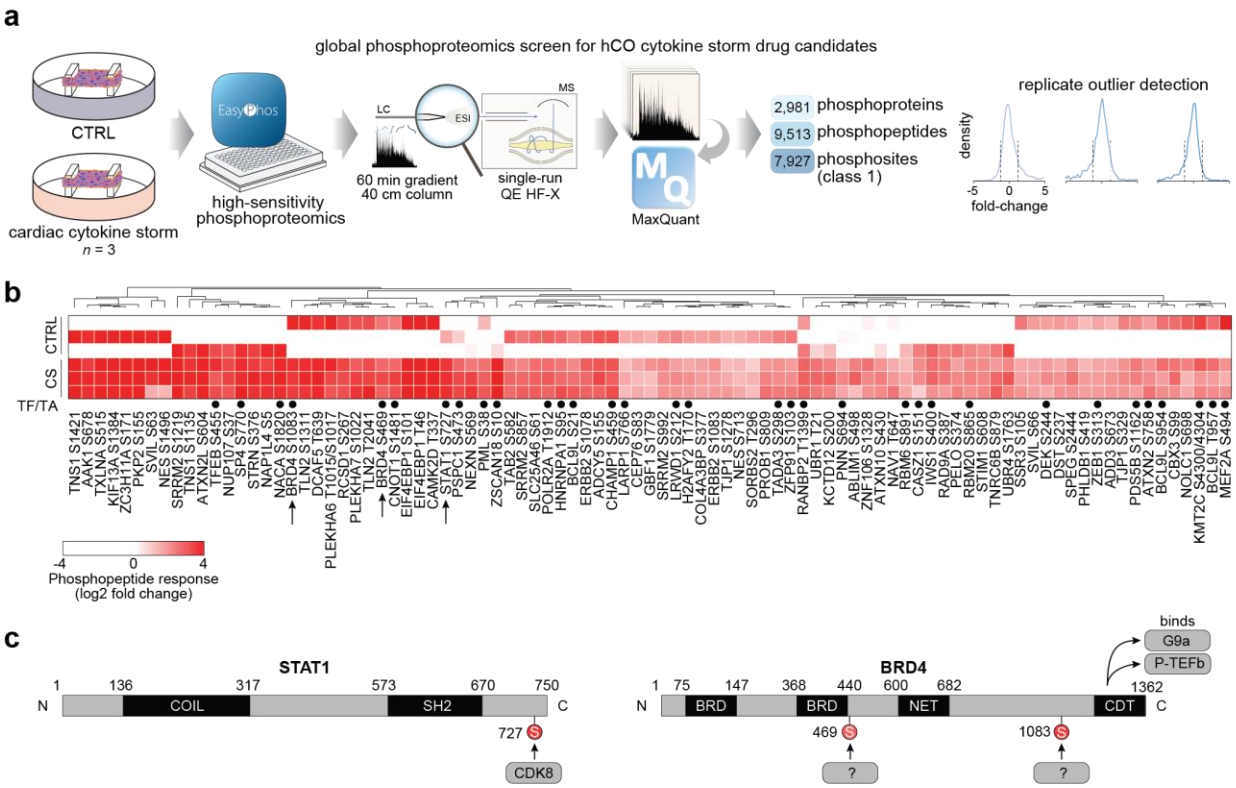

Figure 2: Phophosproteomics reveals signalling driving cardiac dysfunction.

a) Schematic of the experiment and analysis
b) Heat-map of enriched phosphopeptides in hCO following cardiac cytokine storm treatment (after 1 hour). TF/TA circles depict transcription factors and transcriptional activators.
c) Phosphorylation sites induced by cardiac cytokine storm on STAT1 and BRD4.

hPSC cardiac cells- AA, Endothelial cells- RM3.5.

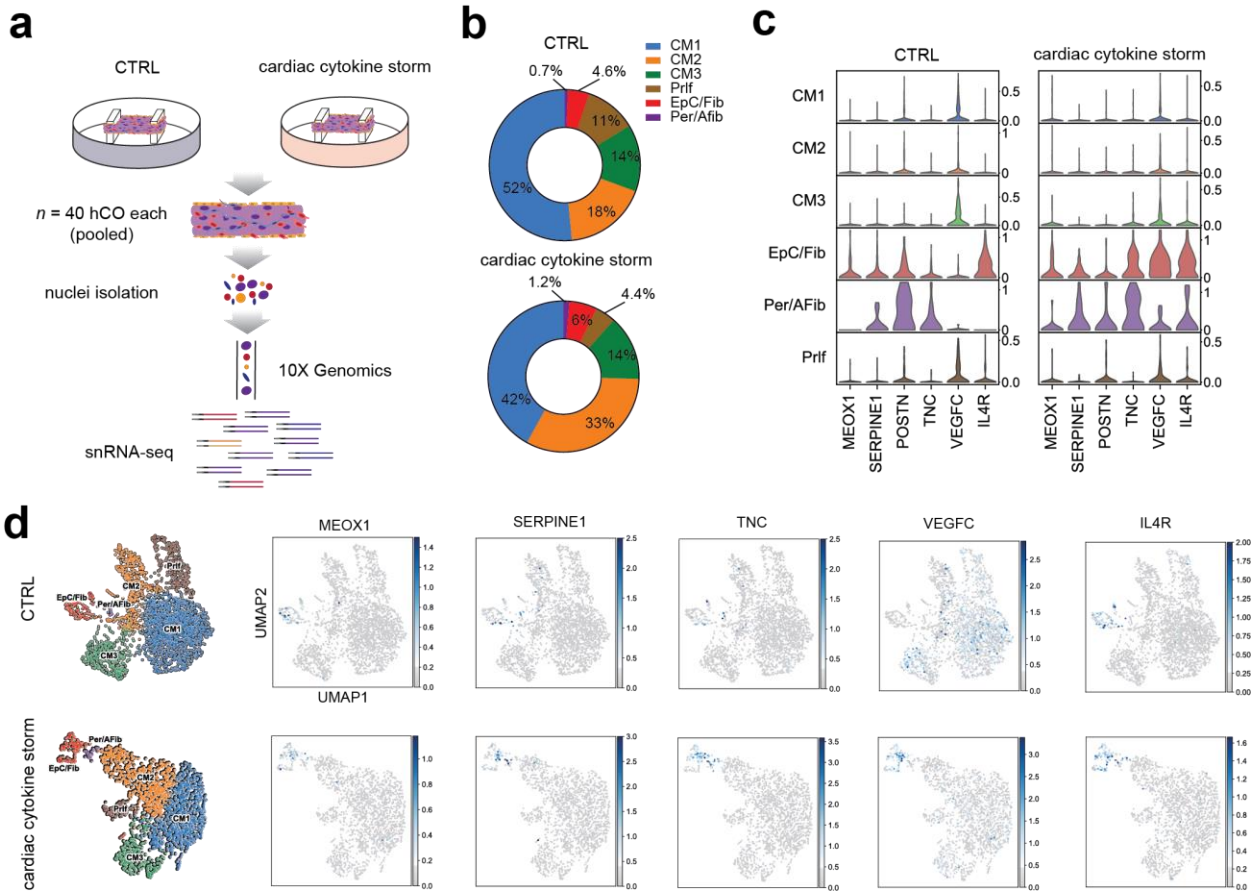

Figure 3: snRNA-seq reveals that cytokine storm activates fibroblasts in hCO

a) Schematic of experiment
b) Cell compositions identified in snRNA-seq
c) Expression level of fibroblast activation markers
d) UMAP of CTRL and cytokine storm treated hCO subpopulations and activated fibroblast markers

hPSC cardiac cells- HES3, Endothelial cells- RM3.5. CM – cardiomyocyte, Prlf – proliferating, EpC – epicardial cells, Fib – fibroblasts, Per – pericytes, Afib – activated fibroblasts.

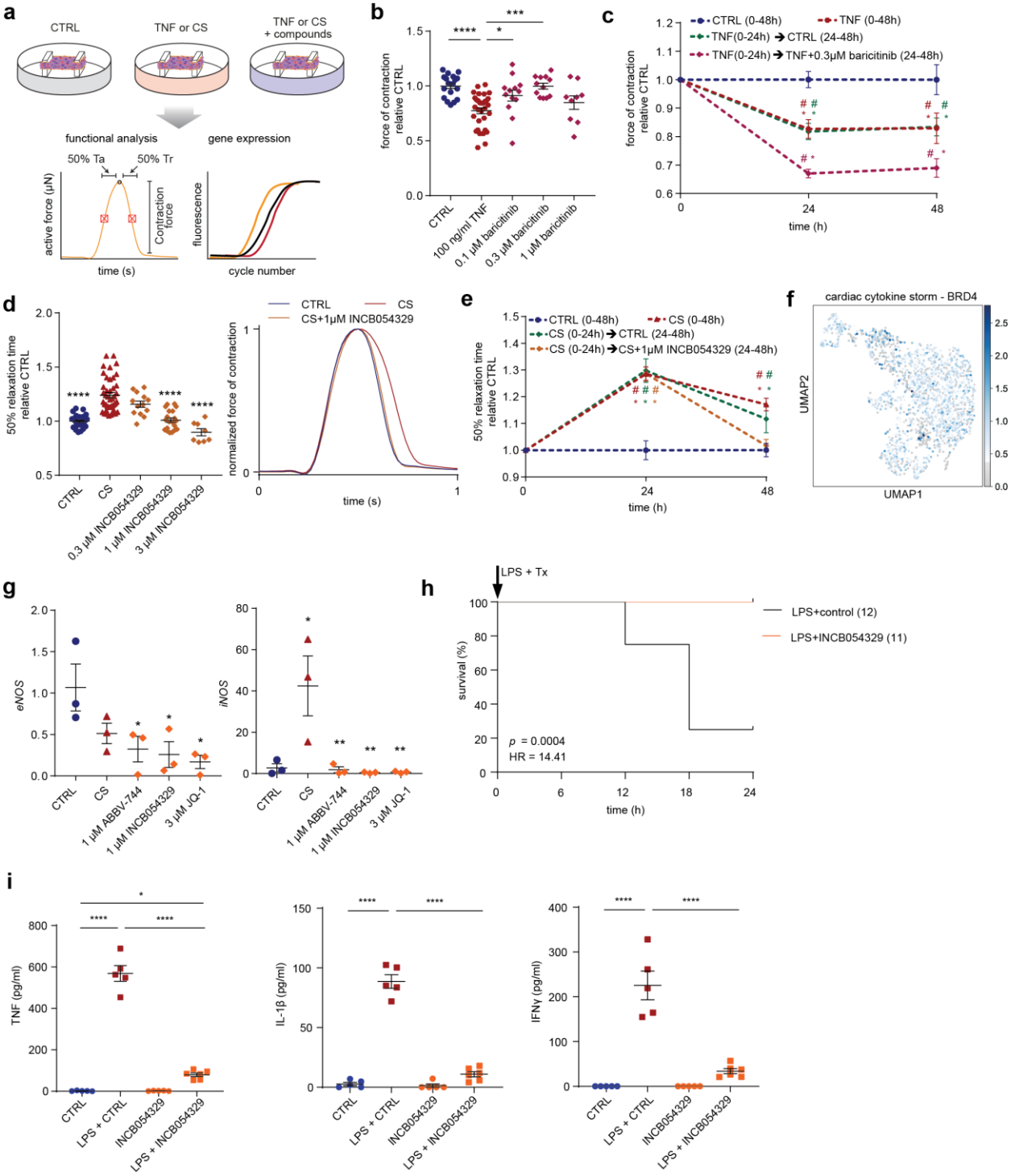

Figure 4: BRD4 inhibition using INCB054329 improves cardiac function and prevents death in sepsis models

a) Schematic of experiment
b) Protection against systolic dysfunction (force of contraction) by baricitinib. n = 9-32 hCOs per condition from 2-3 experiments. *p<0.05, *** p<0.001, **** p<0.0001 using one-way ANOVA with Dunnett's multiple comparisons test,

c) Assessment of hCO recovery from TNF and baricitinib treatment. n = 6-7 hCOs per condition from 1 experiment. # $p<0.05$ compared to CTRL at the same time-point, and * $p<0.05$ compared to specific condition at 0 h with colour indicating comparison, using two-way ANOVA with Dunnett's multiple comparisons test.
d) Protection against diastolic dysfunction (time to 50% relaxation time) by INCB054329. n = 8-43 hCOs per condition from 2-4 experiments. *$p<0.05$, *** $p<0.001$, **** $p<0.0001$, using one-way ANOVA with Dunnett's multiple comparisons test compared to cardiac cytokine storm.
e) Assessment of hCO recovery from cardiac cytokine storm and INCB054329 treatment. n = 6-7 hCOs per condition from 1 experiment. # $p<0.05$ compared to CTRL at the same time-point, and * $p<0.05$ compared to specific condition at 0 h with colour indicating comparison, using two-way ANOVA with Dunnett's multiple comparisons test.
f) BRD4 is expressed in all cell-populations in hCO
g) BRD4 inhibition prevents cardiac cytokine storm induced iNOS in hCO. n = 3 (2 pooled hCO) from 1 experiment. * $p<0.05$ and ** $p<0.01$, using a one-way ANOVA with Tukey's multiple comparisons test.
h) Kaplan-Meier curve of survival after LPS injection. n = 12 control and 11 INCB054329 treatment (67 mg/kg). P-value calculated using Gehan-Breslow-Wilcoxon test.
i) Cytokine levels 6 h after LPS. n = 5-6 mice. **** $p<0.0001$, using one-way ANOVA with Tukey's multiple comparisons test.

hPSC cardiac cells- HES3, Endothelial cells- RM3.5.

METHODS

Mice

Wild-type (WT) C57BL/6 were purchased from Walter and Eliza Hall Institute for Medical Research or bred in house at QIMR Berghofer Medical Research Institute. Mice used in this study were older than 6 weeks and were sex-matched. The number of mice in each group of treatment for each experiment is indicated in the figure legends. In all studies, no mice were excluded based on pre-established criteria and randomization was applied immediately prior to treatment in therapy experiments. Experiments were conducted as approved by the QIMR Berghofer Medical Research Institute Animal Ethics Committee.

Cell lines

Ethical approval for the use of human embryonic stem cells (hESCs) was obtained from QIMR Berghofer's Ethics Committee and was carried out in accordance with the National Health and Medical Research Council of Australia (NHMRC) regulations. hESCs utilized were female HES3 (WiCell), and male RM3.5 iPSC line (generated by Edouard Stanley (Murdoch Children's Research Institute, Melbourne, Australia)). The following cell lines were obtained from the CIRM hPSC Repository funded by the California Institute of Regenerative Medicine: CW30382A (male, designated AA) and CW30318C (female, designated CC) which were both obtained from FujiFilm. hPSC lines were maintained in mTeSR-1 (Stem Cell Technologies)/Matrigel (Millipore) and passaged using TrypLE (ThermoFisher Scientific) or ReLeSR (Stem Cell Technologies). Quality control was performed with Karyotyping and mycoplasma testing.

Cardiac differentiation

Cardiac differentiation was performed as previously described[13,15,51]. hPSCs were seeded on Matrigel-coated flasks at 2 x 10^4 cells/cm^2 and cultured in mTeSR-1 for 4 days. To induce cardiac mesoderm, hPSCs were cultured in RPMI B27-medium (RPMI 1640 GlutaMAX+ 2% B27 supplement without insulin, 200 µM L-ascorbic acid 2-phosphate sesquimagnesium salt hydrate (Sigma) and 1% Penicillin/Streptomycin (ThermoFisher Scientific), supplemented with 5 ng/ml BMP-4 (RnD Systems), 9 ng/ml Activin A (RnD Systems), 5 ng/ml FGF-2 (RnD Systems) and 1 µM CHIR99021 (Stem Cell Technologies). Mesoderm induction required daily medium exchanges for 3 days. This was followed by cardiac specification using RPMI B27- containing 5 µM IWP-4 (Stem Cell Technologies) for another 3 days, and then further 7 days using 5 µM IWP-4 RPMI B27+ (RPMI1640 Glutamax + 2% B27 supplement with insulin, 200 µM L-ascorbic acid 2-phosphate sesquimagnesium salt hydrate and 1% Penicillin/Streptomycin) with media change every 2-3 days. For the final 2 days of differentiation, hPSCs were cultured in RPMI B27+. Harvest of differentiated cardiac cells involved enzymatic digestion, firstly in 0.2% collagenase type I (Sigma) containing 20% fetal bovine serum (FBS) in PBS (with Ca^{2+} and Mg^{2+}) at 37°C for 1 h, and secondly in 0.25% trypsin-EDTA at 37°C for 10 minutes. Cells were filtered through a 100 µm mesh cell strainer (BD Biosciences), centrifuged at 300 x g for 3 minutes, and resuspended in α-MEM Glutamax, 10% FBS, 200 µM L-ascorbic acid 2-phosphate sesquimagnesium salt hydrate and 1% Penicillin/Streptomycin. Previous flow cytometry analysis indicated that differentiated cardiac cells were ~70% α-actinin$^+$/CTNT$^+$ cardiomyocytes, ~30% CD90 stromal cells[15].

Endothelial differentiation

Endothelial cell differentiation was performed following a protocol modified from[52]. hPSCs were seeded onto Matrigel-coated T-25 or T-75 tissue culture flasks at the density 5 x 10^3 cells/cm^2 and cultured in mTeSR-1 for 3 days. Mesoderm was induced with RPMI B27- (RPMI 1640 GlutaMAX+ 2% B27 supplement without insulin, 200 µM L-ascorbic acid 2-phosphate sesquimagnesium salt hydrate (Sigma) and 1% Penicillin/Streptomycin (ThermoFisher Scientific), and the small molecules 25 ng/ml Activin A (R&D systems), 30 ng/ml Bone morphogenic protein-4 (BMP4) (R&D systems), 1.5 µM CHIR99021 (Stemgent), and 50 ng/ml Vascular Endothelial Growth Factor type A (VEGF-A) (Peprotech) for 3 days (no media changes). Endothelial cell fate was further specified with RPMI B27- medium supplemented with 50 ng/ml VEGF-A and 10 µM SB431542 with media changes every 2 to 3 days until day 8.

FACS sorting endothelial cells

Endothelial cells were harvested on day 8 of differentiation using TrypLE (ThermoFisher Scientific). Single cells were separated using a 100 µm strainer and labelled with CD31 antibody (1:200, M082329-2, DAKO) at 4°C for 45 minutes followed by 30 min staining with a goat anti-mouse secondary antibody conjugated to AlexaFluor 488 or 555 (1:400, A-11001 and A-21422, ThermoFisher Scientific). Cells were analysed using Becton Dickinson FACSAria II, gated on forward and side scatter. Single cells were identified and sorted based on CD31+ expression. CD31+ endothelial cells were expanded in EGM-2 (Lonza) in Matrigel flasks and cryopreserved.

hCO fabrication

hCO culture inserts were fabricated using SU-8 photolithography and PDMS molding[13]. Differentiated cells were mixed at ratio of 20% endothelial cells and 80% cardiomyocytes/fibroblasts to form hCO. Acid-solubilized bovine collagen 1 (Devro) was salt balanced using 10x DMEM (ThermoFisher Scientific) and pH neutralized using 0.1M NaOH before combining with Matrigel and then the cell suspension on ice. Each hCO contained 5 x 10^4 cells, a final concentration of 2.6 mg/ml collagen I and 9% Matrigel. 3.5 µL of suspension was pipetted into the hCO culture insert and incubated at 37°C with 5% CO_2 for 45 min in order to gel. After gelling, α-MEM GlutaMAX (ThermoFisher Scientific), 10% fetal bovine serum (FBS), 200 µM L-ascorbic acid 2-phosphate sesquimagnesium salt hydrate (Sigma) and 1% Penicillin/Streptomycin (ThermoFisher Scientific) was added. hCO were subsequently cultured in maturation media[13] with medium changes every 2 to 3 days for 5 days (7 days old hCO). To better approximate adult metabolic provisions a 'weaning medium' (WM) was utilized. hCO were cultured in WM containing 4% B27 – insulin, 5.5 mM glucose, 1 nM insulin, 200 µM L-ascorbic acid 2-phosphate sesquimagnesium salt hydrate, 1% P/S, 1% GlutaMAX (100x), 33 µg/mL aprotinin and 10 µM palmitate (conjugated to bovine serum albumin in B27) in DMEM without glucose, glutamine and phenol red (ThermoFisher Scientific) with media changes every 2-3 days.

Force analysis of hCO

The elasticity of the Heart Dyno poles enables the contractile properties to be determined via tracking pole deflection, which directly correlates with force[13]. Videos of 10 seconds were made of each hCO with the Nikon ANDOR WD Revolution Spinning Disk microscope (magnification 4x). While imaging, hCO were incubated at 37°C, 5% CO_2 to prevent changes in contractile behaviour. For pacing, hCOs were electrically stimulated at 1 Hz with 5ms square pulses with 20 mA current using a Panlab/Harvard Apparatus Digital Stimulator. Videos were then analysed with a custom written Matlab program[13]. This facilitated the analysis of the contractile properties of the organoids and the production of time-force graphs[13]. Moreover, data was obtained regarding

additional important functional parameters including the contraction rate and the activation and relaxation time of the organoids.

Immunostaining of hCO

hCO were fixed with 1% paraformaldehyde (Sigma) for 1 h. Cells were stained with primary antibodies CD31 (1:200, M082329-2, DAKO), NG2 (1:200, 14-6504-82, ThermoFisher Scientific) and cardiac troponin T (1;400, ab45932, Abcam) in 5% FBS and 0.25% TritonX-100 Blocking Buffer at 4°C overnight on a rocker. Cells were washed twice for 1 h with Blocking Buffer and labelled with secondary antibodies goat anti-mouse IgG_1 AlexaFluor 488 (1:400, A-21121), goat anti-mouse IgG_{2a} AlexaFluor 555 (1:400, A-21137) and goat anti-rabbit AlexaFluor 633 (1:400, A-21070) and Hoechst3332 (all ThermoFisher Scientific) at 4°C overnight on a rocker. Cells were again washed with Blocking Buffer twice for 1 h and mounted on microscope slides using ProLong Glass (ThermoFisher Scientific).

Phospho-proteomics

Phosphoproteomics experiments were performed with biological triplicates. Phosphopeptides were enriched from 20 pooled human cardiac organoids, yielding approximately 100 µg of total protein per condition. The high-sensitivity EasyPhos workflow was employed as previously described[24]. Briefly, pooled organoids were lysed in SDC buffer (4% Sodium deoxycholate, 100 mM Tris pH 8.5) and immediately heated for 5 min at 95°C. Lysates were cooled on ice, and sonicated with a tip-probe sonicator (50% output power, 30 seconds). An aliquot of lysate was taken and diluted 1:5 in 8M Urea from which protein concentration was determined by BCA assay (Thermo Fisher Scientific). Aliquots corresponding to 100 µg of protein were subsequently diluted in SDC buffer into a 96-well deep-well plate, reduced and alkylated at 45°C for 5 min by the addition of 10 mM Tris (2-carboxyethyl)phosphine (TCEP)/40 mM 2-Chloroacetamide (CAA) pH 8, and digested by the addition of 1:100 Lys-C and Trypsin overnight at 37°C with agitation (1,500 rpm). After digestion phosphopeptides were enriched in parallel according to the EasyPhos workflow as described[24]. Eluted phosphopeptides were dried in a SpeedVac concentrator (Eppendorf) and resuspended in MS loading buffer (0.3% TFA/2% acetonitrile) prior to LC-MS/MS measurement.

LC-MS/MS Measurement

Phosphopeptides were loaded onto a 40 cm column fabricated in-house with 75 µM inner diameter fused silica packed with 1.9 µM C18 ReproSil particles (Dr. Maisch GmBH). A column oven (Sonation) was used to maintain column temperature at 60°C, and a U3000 HPLC system (Dionex, Thermo Fisher Scientific) was connected to a Q Exactive HF X benchtop Orbitrap mass spectrometer (Thermo Fisher Scientific) with a NanoSpray Flex ion source (Thermo Fisher Scientific). For all samples, peptides were separated using a binary buffer system of 0.1% (v/v) formic acid (buffer A) and 80% (v/v) acetonitrile/0.1% (v/v) formic acid (buffer B). Peptides were eluted at a flow rate of 400 nL/min and separated with a gradient of 3 – 19% buffer B over 40 minutes, followed by 19 – 41% buffer B over 20 minutes, and peptides were analysed with a full scan (350 – 1,400 m/z; R=60,000 at 200 m/z) at a target of 3e6 ions, followed by up to ten data-dependent MS2 scans using HCD (target 1e5; max. IT 50 ms; isolation window 1.6 m/z; NCE 27%; min. AGC target 2e4), detected in the Orbitrap mass analyser (R=15,000 at 200 m/z). Dynamic exclusion (30 s) and Apex trigger (2 to 4 s) were enabled.

MS data processing

RAW MS data was processed in the MaxQuant software environment[53] (version 1.6.0.9), searching against the Human UniProt Reference database (December 2019 release), using default settings with the addition of 'Phospho(STY)' as a variable modification and 'Match between runs' switched on for all analyses. Data analysis was performed using the Perseus software package[54].

Single nuclei RNA-sequencing of hCO

Pooled hCO (~40) were homogenized in 4 mL lysis buffer (300 mM sucrose, 10 mM Tris-HCl (pH = 8), 5 mM $CaCl_2$, 5 mM magnesium acetate, 2 mM EDTA, 0.5 mM EGTA, 1 mM DTT)(all Sigma-Aldrich) with 30 strokes of a dounce tissue grinder (Wheaton). Large pieces of hCO were allowed to settle and homogenate was passed through pre-wetted 40 µm cell strainers (Becton Dickinson). Remaining hCO material in the douncer was resuspended in 4 mL and the douncing and filtering steps were repeated twice. All steps of the homogenization were performed on ice. The filtered homogenate was centrifuged at 1500 x g for 5 min at 4ºC. Nuclei pellets were then re-suspended in PBS. A fraction of resuspended nuclei were then stained with hoechst nuclear stain (1:500 dilution) and counted on a haemocytometer under fluorescent microscope.

The nuclei were then re-centrifuged (1500 x g for 5 min at 4°C) and resuspended at a density to load ~5,000 nuclei per sample. Cell were loaded into the Chromium Controller (10X Genomics) for gel bead emulsion (GEM) formation. Library preparation was conducted according to the manufacturer's recommended protocol using the Chromium Next GEM Single Cell 3' GEM, Library & Gel Bead Kit v3.1. Libraries were sequenced on the NextSeq 500/550 v2 (Illumina) with 150 bp reads and were sequenced to ~250,000 reads per cell.

Raw fastq reads for each sample were processed using CellRanger v3.1.0. Default options were used with CellRanger and a custom made pre mRNA reference using GRCh38 v3.0.0 was used to map the reads and for count quantification with the CellRanger counts tool. Following this, the counts were then aggregated together to create a single matrix that contained all the samples. Reads from the single nuclei sequencing data were aligned to a human pre-mRNA GRCh38 reference genome. All pre-processing and filtering steps of the datasets were subsequently carried out via the Python package Scanpy (https://scanpy.readthedocs.io/en/stable/)[55]. Briefly, there was an initial filtering step for genes that are expressed in 3 or more cells and cells with at least 200 detected genes, subsequently removing cells displaying high expression of mitochondrial genes using a cut-off of 4%. We then filtered out cells that had a count depth with a threshold of under 2,000 and higher than 40,000 to remove debris and potential doublets. Gene expression was subsequently normalized for each cell by total expression, scaled by 10,000 and log scaled. Highly variable genes were then identified for clustering. Leiden clustering with an initial resolution of 0.2 was performed to identify clusters within the data. A published human cardiac snRNA-seq dataset was then used to identify overlap of marker gene sets for main human heart cell types (e.g. cardiomyocytes, fibroblasts, epicardium, pericytes, etc) with the clusters of our dataset, and were labelled accordingly[17]. Further refined clustering was carried out on specific clusters that showed overlap of more than one of the various heart cell types. Visualization of the datasets was primarily carried out using nonlinear dimensionality reduction UMAP plots[56]. In the snRNA-seq we note the lower than expected percentage of non-myocytes and the loss of endothelial cells[13,15], indicating the protocol requires further optimization for hCO samples.

hCO comparison to bulk nuclei RNA sequencing data for PCA

Nuclear RNA-seq dataset generated from sorted cardiomyocyte nuclei at two stages (fetal and adult) was obtained from BioProject ID: PRJNA353755[18]. RNA-seq dataset was mapped to the human genome (hg38) using STAR aligner (version 2.7.3a). Annotations and genome files (hg38) were obtained from *Ensembl*. Uniquely mapped reads were counted across genes with a program in Bioconductor R[57] package, featureCounts (version 2.0.1)[58]. Subsequent analyses of the count data were performed in the R statistical programming language with the Bioconductor packages edgeR[59] and the annotation package org. Hs.eg.db. In this dataset, genes were retained for statistical analysis if they were expressed at a count per million (CPM) above 0.5 in at least 4 samples. Additionally, ribosomal and mitochondrial genes as well as pseudogenes, and genes with no annotation (Entrez Gene identification) were removed before normalization and statistical analysis.

Principal component analysis (PCA) performed using the intersection of the 25% most highly variable genes of the snRNA-seq dataset and genes expressed in the bulk samples. Each of the two datasets were log transformed and scaled separately before running the dimensionality reduction method.

Pro-inflammatory stimulation of hCO

Cytokines (human) and factors were added individually and in combinations in WM: 100 ng/ml TNF, 10 ng/ml IL-1β, 100 ng/ml IFN-γ, 100 ng/ml IL-6, 100 ng/ml IL-17A, 100 ng/ml G-CSF (Amgen), 10 µg/ml poly(I:C) (HMW, Invivogen) or 1 µg/ml LPS (from *Escherichia coli* strain 0127:B8, Sigma) (all Peprotech unless noted). Additional concentrations were performed for the dose-response curves for TNF, IL-1β, IFN-γ and poly(I:C) as indicated. The function of hCO was determined before addition of these factors as a baseline (time 0 h) and any changes normalized to the original baseline and to the control. The medium was not exchanged unless noted.

Drug screening

Compounds were sources from MedChem Express (unless noted) and dissolved at 10 mM in DMSO and vehicle controls used. A larger batch of INCB054329 was sourced from Selleckchem. The following compounds were used at 2 or 3 doses previously shown to have *in vitro* efficacy as per the reference papers for: JQ-1 (Selleckchem), INCB054329, ABBV-744, ruxolitinib, baricitinib, flavopiridol, SEL120-34A, BI-1347, and paroxetine hydrochloride. Compounds were given at the time of pro-inflammatory factor addition, except for experiments with baricitnib and INCB054329 where recovery of function was also assessed by addition 24 h following addition of inflamatory factors.

Linear regression of cytokine storm responses

To determine factor effects, second order OLS linear regression was performed across all relevant samples using binary predictors (cytokine presence/absence) with force, relaxation/activation times as the outcome variables. p-values were determined using two-tailed t-tests. Normality (Shipiro-Wilks), heteroskedasticity (Breusch-Pagan), linearity (Harvey-Collier), multicollinearity (condition no.) and skewness/kurtosis (Jarque-Bera) were all checked with the respective tests. The coefficient of determination, R^2 (adjusted), was used to determine goodness of fit.

Quantitative RT-PCR

RNA was extracted using QIAGEN RNAeasy Micro Kits (Qiagen). cDNA synthesis using Superscript III (ThermoFisher Scientific) was carried out as per manufacturer's instructions. Final primer concentration of 200-250 nM was used and gene expression was assessed over 40 cycles on an Applied Biosciences Quant Studio 5. Gene expression analysis was normalized to control hCO using the 2^-(ddCT) method. *HPRT1* or *hprt* were used for normalization as a low expressed house-keeping control. Undetected candidate genes (which occurred in some samples for the very low expressed genes *NOS2* and *NOS3*) were assigned cycle number 41. Primers:

<u>Human</u>

HPRT1: Fwd 5' AACCTCTCGGCTTTCCCG Rev 5' TCACTAATCACGACGCCAGG

NOS2: Fwd 5' ACCTTTGATGAGGGGACTGG Rev 5' GTTCTTCACTGTGGGGCTTG

NOS3 Fwd 5' CCGGAACAGCACAAGAGTTA Rev 5' CCCTGCACTGTCTGTGTTAC

<u>Mouse</u>

Hprt Fwd 5' AGGCCAGACTTTGTTGGATTTGAA Rev 5' CAACTTGCGCTCATCTTAGGCTTT

Meox1 Fwd 5' TTTGCCCACCACAACTACCT Rev 5' CAGACTTTGACCTGCCGCT

Tnc Fwd 5' CATCTCAGGGCTTCCACCTA Rev 5' GGCAAGGCCTCTGTGGTA

Nos2 Fwd 5' CTCTAGTGAAGCAAAGCCCA Rev 5' CTCACATACTGTGGACGGG

Nos3 Fwd 5' GAGGCAATCTTCGTTCAGCC Rev 5' ATAGCCCGCATAGCGTATCA

Mouse LPS cytokine storm model

LPS (from *Escherichia coli* strain 0127:B8, Sigma) suspended in PBS was injected intraperitoneally into mice at 0.6 mg per 30 g mouse body weight. After the injection of LPS mice were randomized and received either vehicle 30% (m/v) Kolliphor 15 HS (Sigma) in PBS or 2 mg per 30 g mouse body weight of INCB054329 at 20 mg/kg in the Kolliphor solution. Treatment groups were blinded. For survival experiments, mice were checked hourly for signs of sepsis.

Serum cytokine assays

Serum cytokine levels (IFN-γ, IL-1β and TNF) were determined with a CBA Flex Set Multiplex Cytokine Bead Array (BD Biosciences).

Data reproducibility and statistical analysis

hCO force experiments were performed on quality controlled hCO (proper formation around the poles, non-arrhythmic, no broken arms, no necking[13]) across multiple experiments with multiple cell line combinations to ensure reproducibility. Automated force analysis removes the requirement for blinding of hCO experiments. Personnel performing the animal experiments and analyses were blinded to the conditions or treatments. Statistics were performed using GraphPad Prism v8 unless noted.

REFERENCES

1 Guo, T. *et al.* Cardiovascular Implications of Fatal Outcomes of Patients With Coronavirus Disease 2019 (COVID-19). *JAMA Cardiology* **5**, 811-818, doi:10.1001/jamacardio.2020.1017 (2020).

2 Wu, Z. & McGoogan, J. M. Characteristics of and Important Lessons From the Coronavirus Disease 2019 (COVID-19) Outbreak in China: Summary of a Report of 72 314 Cases From the Chinese Center for Disease Control and Prevention. *JAMA* **323**, 1239-1242, doi:10.1001/jama.2020.2648 (2020).

3 Shi, S. *et al.* Association of Cardiac Injury With Mortality in Hospitalized Patients With COVID-19 in Wuhan, China. *JAMA Cardiology* **5**, 802-810, doi:10.1001/jamacardio.2020.0950 (2020).

4 Chen, C., Li, H., Hang, W. & Wang, D. W. Cardiac injuries in coronavirus disease 2019 (COVID-19). *Journal of Molecular and Cellular Cardiology* **145**, 25-29, doi:10.1016/j.yjmcc.2020.06.002 (2020).

5 Gupta, A. *et al.* Extrapulmonary manifestations of COVID-19. *Nature Medicine* **26**, 1017-1032, doi:10.1038/s41591-020-0968-3 (2020).

6 Goyal, P. *et al.* Clinical Characteristics of Covid-19 in New York City. *New England Journal of Medicine* **382**, 2372-2374, doi:10.1056/NEJMc2010419 (2020).

7 Szekely, Y. *et al.* The Spectrum of Cardiac Manifestations in Coronavirus Disease 2019 (COVID-19) - a Systematic Echocardiographic Study. *Circulation* **0**, doi:doi:10.1161/CIRCULATIONAHA.120.047971 (2020).

8 Puntmann, V. O. *et al.* Outcomes of Cardiovascular Magnetic Resonance Imaging in Patients Recently Recovered From Coronavirus Disease 2019 (COVID-19). *JAMA Cardiology*, doi:10.1001/jamacardio.2020.3557 (2020).

9 Feldman, A. M. *et al.* The role of tumor necrosis factor in the pathophysiology of heart failure. *Journal of the American College of Cardiology* **35**, 537-544, doi:10.1016/s0735-1097(99)00600-2 (2000).

10 Horby, P. *et al.* Effect of Dexamethasone in Hospitalized Patients with COVID-19: Preliminary Report. *medRxiv*, 2020.2006.2022.20137273, doi:10.1101/2020.06.22.20137273 (2020).

11 Mangalmurti, N. & Hunter, C. A. Cytokine Storms: Understanding COVID-19. *Immunity* **53**, 19-25, doi:https://doi.org/10.1016/j.immuni.2020.06.017 (2020).

12 Mills, R. J. *et al.* Drug Screening in Human PSC-Cardiac Organoids Identifies Pro-proliferative Compounds Acting via the Mevalonate Pathway. *Cell stem cell* **24**, 895-907.e896, doi:10.1016/j.stem.2019.03.009 (2019).

13 Mills, R. J. *et al.* Functional screening in human cardiac organoids reveals a metabolic mechanism for cardiomyocyte cell cycle arrest. *Proceedings of the National Academy of Sciences* **114**, E8372-E8381, doi:10.1073/pnas.1707316114 (2017).

14 Huang, C. *et al.* Clinical features of patients infected with 2019 novel coronavirus in Wuhan, China. *The Lancet* **395**, 497-506, doi:https://doi.org/10.1016/S0140-6736(20)30183-5 (2020).

15 Voges, H. K. *et al.* Development of a human cardiac organoid injury model reveals innate regenerative potential. *Development (Cambridge, England)* **144**, 1118-1127, doi:10.1242/dev.143966 (2017).

16 Quaife-Ryan, G. A. *et al.* Multicellular Transcriptional Analysis of Mammalian Heart Regeneration. *Circulation* **136**, 1123-1139, doi:10.1161/circulationaha.117.028252 (2017).

17 Tucker, N. R. *et al.* Transcriptional and Cellular Diversity of the Human Heart. *Circulation* **0**, doi:doi:10.1161/CIRCULATIONAHA.119.045401 (2020).

18 Gilsbach, R. *et al.* Distinct epigenetic programs regulate cardiac myocyte development and disease in the human heart in vivo. *Nature communications* **9**, 391, doi:10.1038/s41467-017-02762-z (2018).
19 Vasudevan, N. T. *et al.* Gβγ-independent recruitment of G-protein coupled receptor kinase 2 drives tumor necrosis factor α-induced cardiac β-adrenergic receptor dysfunction. *Circulation* **128**, 377-387, doi:doi:10.1161/CIRCULATIONAHA.113.003183 (2013).
20 Kubota, T. *et al.* Dilated Cardiomyopathy in Transgenic Mice With Cardiac-Specific Overexpression of Tumor Necrosis Factor-&#x3b1. *Circulation research* **81**, 627-635, doi:doi:10.1161/01.RES.81.4.627 (1997).
21 Levick, S. P. & Goldspink, P. H. Could interferon-gamma be a therapeutic target for treating heart failure? *Heart failure reviews* **19**, 227-236, doi:10.1007/s10741-013-9393-8 (2014).
22 Needham, E. J., Parker, B. L., Burykin, T., James, D. E. & Humphrey, S. J. Illuminating the dark phosphoproteome. *Science Signaling* **12**, eaau8645, doi:10.1126/scisignal.aau8645 (2019).
23 Humphrey, S. J., Azimifar, S. B. & Mann, M. High-throughput phosphoproteomics reveals in vivo insulin signaling dynamics. *Nature biotechnology* **33**, 990-995, doi:10.1038/nbt.3327 (2015).
24 Humphrey, S. J., Karayel, O., James, D. E. & Mann, M. High-throughput and high-sensitivity phosphoproteomics with the EasyPhos platform. *Nature Protocols* **13**, 1897-1916, doi:10.1038/s41596-018-0014-9 (2018).
25 Alexanian, M. *et al.* A Transcriptional Switch Governing Fibroblast Plasticity Underlies Reversibility of Chronic Heart Disease. *bioRxiv*, 2020.2007.2021.214874, doi:10.1101/2020.07.21.214874 (2020).
26 Hahn, V. S. *et al.* Endomyocardial Biopsy Characterization of Heart Failure With Preserved Ejection Fraction and Prevalence of Cardiac Amyloidosis. *JACC: Heart Failure*, doi:https://doi.org/10.1016/j.jchf.2020.04.007 (2020).
27 Schumacher, S. M. *et al.* Paroxetine-mediated GRK2 inhibition reverses cardiac dysfunction and remodeling after myocardial infarction. *Science translational medicine* **7**, 277ra231-277ra231, doi:10.1126/scitranslmed.aaa0154 (2015).
28 Guo, S., Carter, R. L., Grisanti, L. A., Koch, W. J. & Tilley, D. G. Impact of paroxetine on proximal β-adrenergic receptor signaling. *Cell Signal* **38**, 127-133, doi:10.1016/j.cellsig.2017.07.006 (2017).
29 Evron, T., Daigle, T. L. & Caron, M. G. GRK2: multiple roles beyond G protein-coupled receptor desensitization. *Trends Pharmacol Sci* **33**, 154-164, doi:10.1016/j.tips.2011.12.003 (2012).
30 Richardson, P. *et al.* Baricitinib as potential treatment for 2019-nCoV acute respiratory disease. *Lancet* **395**, e30-e31, doi:10.1016/S0140-6736(20)30304-4 (2020).
31 Sadzak, I. *et al.* Recruitment of Stat1 to chromatin is required for interferon-induced serine phosphorylation of Stat1 transactivation domain. *Proceedings of the National Academy of Sciences of the United States of America* **105**, 8944-8949, doi:10.1073/pnas.0801794105 (2008).
32 Bancerek, J. *et al.* CDK8 kinase phosphorylates transcription factor STAT1 to selectively regulate the interferon response. *Immunity* **38**, 250-262, doi:10.1016/j.immuni.2012.10.017 (2013).
33 Rzymski, T. *et al.* SEL120-34A is a novel CDK8 inhibitor active in AML cells with high levels of serine phosphorylation of STAT1 and STAT5 transactivation domains. *Oncotarget* **8**, 33779-33795, doi:10.18632/oncotarget.16810 (2017).
34 Hofmann, M. H. *et al.* Selective and Potent CDK8/19 Inhibitors Enhance NK-Cell Activity and Promote Tumor Surveillance. *Molecular Cancer Therapeutics* **19**, 1018-1030, doi:10.1158/1535-7163.mct-19-0789 (2020).
35 Stubbs, M. C. *et al.* The Novel Bromodomain and Extraterminal Domain Inhibitor INCB054329 Induces Vulnerabilities in Myeloma Cells That Inform Rational Combination Strategies. *Clinical Cancer Research* **25**, 300-311, doi:10.1158/1078-0432.ccr-18-0098 (2019).

36 Filippakopoulos, P. *et al.* Selective inhibition of BET bromodomains. *Nature* **468**, 1067-1073, doi:10.1038/nature09504 (2010).
37 Faivre, E. J. *et al.* Selective inhibition of the BD2 bromodomain of BET proteins in prostate cancer. *Nature* **578**, 306-310, doi:10.1038/s41586-020-1930-8 (2020).
38 Gagliano-Jucá, T. *et al.* Androgen Deprivation Therapy Is Associated With Prolongation of QTc Interval in Men With Prostate Cancer. *J Endocr Soc* **2**, 485-496, doi:10.1210/js.2018-00039 (2018).
39 Huang, L. *et al.* Cardiac Involvement in Patients Recovered From COVID-2019 Identified Using Magnetic Resonance Imaging. *JACC: Cardiovascular Imaging*, 3427, doi:10.1016/j.jcmg.2020.05.004 (2020).
40 Stratton, M. S. *et al.* Dynamic Chromatin Targeting of BRD4 Stimulates Cardiac Fibroblast Activation. *Circulation research* **125**, 662-677, doi:doi:10.1161/CIRCRESAHA.119.315125 (2019).
41 Stratton, M. S., Haldar, S. M. & McKinsey, T. A. BRD4 inhibition for the treatment of pathological organ fibrosis. *F1000Res* **6**, F1000 Faculty Rev-1015, doi:10.12688/f1000research.11339.1 (2017).
42 Paulus, W. J. & Tschöpe, C. A Novel Paradigm for Heart Failure With Preserved Ejection Fraction: Comorbidities Drive Myocardial Dysfunction and Remodeling Through Coronary Microvascular Endothelial Inflammation. *Journal of the American College of Cardiology* **62**, 263-271, doi:https://doi.org/10.1016/j.jacc.2013.02.092 (2013).
43 Finkel, M. *et al.* Negative inotropic effects of cytokines on the heart mediated by nitric oxide. *Science* **257**, 387-389, doi:10.1126/science.1631560 (1992).
44 Schiattarella, G. G. *et al.* Nitrosative stress drives heart failure with preserved ejection fraction. *Nature* **568**, 351-356, doi:10.1038/s41586-019-1100-z (2019).
45 Runte, K. E. *et al.* Relaxation and the Role of Calcium in Isolated Contracting Myocardium From Patients With Hypertensive Heart Disease and Heart Failure With Preserved Ejection Fraction. *Circ Heart Fail* **10**, doi:10.1161/circheartfailure.117.004311 (2017).
46 Nishiga, M., Wang, D. W., Han, Y., Lewis, D. B. & Wu, J. C. COVID-19 and cardiovascular disease: from basic mechanisms to clinical perspectives. *Nature Reviews Cardiology*, doi:10.1038/s41569-020-0413-9 (2020).
47 Nicodeme, E. *et al.* Suppression of inflammation by a synthetic histone mimic. *Nature* **468**, 1119-1123, doi:10.1038/nature09589 (2010).
48 Duan, Q. *et al.* BET bromodomain inhibition suppresses innate inflammatory and profibrotic transcriptional networks in heart failure. *Science translational medicine* **9**, eaah5084, doi:10.1126/scitranslmed.aah5084 (2017).
49 Cochran, A. G., Conery, A. R. & Sims, R. J. Bromodomains: a new target class for drug development. *Nature Reviews Drug Discovery* **18**, 609-628, doi:10.1038/s41573-019-0030-7 (2019).
50 Falchook, G. *et al.* Abstract A093: Phase 1/2 study of INCB054329, a bromodomain and extraterminal (BET) protein inhibitor, in patients (pts) with advanced malignancies. *Molecular Cancer Therapeutics* **17**, A093-A093, doi:10.1158/1535-7163.targ-17-a093 (2018).
51 Hudson, J., Titmarsh, D., Hidalgo, A., Wolvetang, E. & Cooper-White, J. Primitive cardiac cells from human embryonic stem cells. *Stem cells and development* **21**, 1513-1523, doi:10.1089/scd.2011.0254 (2012).
52 Orlova, V. V. *et al.* Generation, expansion and functional analysis of endothelial cells and pericytes derived from human pluripotent stem cells. *Nature protocols* **9**, 1514-1531, doi:10.1038/nprot.2014.102 (2014).

53 Cox, J. & Mann, M. MaxQuant enables high peptide identification rates, individualized p.p.b.-range mass accuracies and proteome-wide protein quantification. *Nature biotechnology* **26**, 1367-1372, doi:10.1038/nbt.1511 (2008).
54 Tyanova, S. & Cox, J. Perseus: A Bioinformatics Platform for Integrative Analysis of Proteomics Data in Cancer Research. *Methods in molecular biology (Clifton, N.J.)* **1711**, 133-148, doi:10.1007/978-1-4939-7493-1_7 (2018).
55 Wolf, F. A., Angerer, P. & Theis, F. J. SCANPY: large-scale single-cell gene expression data analysis. *Genome biology* **19**, 15, doi:10.1186/s13059-017-1382-0 (2018).
56 Becht, E. *et al.* Dimensionality reduction for visualizing single-cell data using UMAP. *Nature biotechnology* **37**, 38-44, doi:10.1038/nbt.4314 (2019).
57 Huber, W. *et al.* Orchestrating high-throughput genomic analysis with Bioconductor. *Nature methods* **12**, 115-121, doi:10.1038/nmeth.3252 (2015).
58 Liao, Y., Smyth, G. K. & Shi, W. featureCounts: an efficient general purpose program for assigning sequence reads to genomic features. *Bioinformatics (Oxford, England)* **30**, 923-930, doi:10.1093/bioinformatics/btt656 (2014).
59 Robinson, M. D., McCarthy, D. J. & Smyth, G. K. edgeR: a Bioconductor package for differential expression analysis of digital gene expression data. *Bioinformatics (Oxford, England)* **26**, 139-140, doi:10.1093/bioinformatics/btp616 (2010).

ACKNOWLEDGEMENTS

We used the Australian National Fabrication Facility Queensland Node for the fabrication of the Heart-Dyno molds. We thank Grace Chojnowski and Michael Rist for FACS at QIMR Berghofer. Microscopy was aided by Tam Nguyen and Nigel Waterhouse at QIMR Berghofer. Prof Edouard Stanley for provision of the RM3.5 iPSC line (Murdoch Children's Research Institute, Melbourne, Australia). We thank Nadine Shultz and Paul Collins for the sequencing and also Scott Wood and Ross Koufariotis for bioinformatics assistance. We thank Compounds Australia (www.compoundsaustralia.com) for providing access to compounds, however all experiments herein used compounds sourced from MedChem Express or Selleckchem.

We acknowledge grant and fellowship support from the National Health and Medical Research Council of Australia (J.E.H., M.J.S., C.R.E., T.B.), Heart Foundation of Australia (J.E.H.), QIMR Berghofer Medical Research Institute (J.E.H.), The Stafford Fox Foundation (E.R.P.), the Royal Children's Hospital Foundation (E.R.P.), Australian Research Council Strategic Initiative in Stem Cell Science (Stem Cells Australia) (E.R.P. and J.E.H.) and the Medical Research Future Fund (MRFF9200008) (J.E.H., T.B., M.J.S., K.P.A.MD., C.R.E., E.R.P.). M.J.S. is supported by Health and Medical Research Council of Australia Program (APP1132519) and Investigator (APP1173958) grants. The Murdoch Children's Research Institute is supported by the Victorian Government's Operational Infrastructure Support Program.

DECLARATION OF INTERESTS

R.J.M., J.E.H., G.A.Q.-R., D.M.T. and E.R.P. are listed as co-inventors on pending patents held by The University of Queensland and QIMR Berghofer Medical Research Institute that relate to cardiac organoid maturation and putative cardiac regeneration therapeutics. J.E.H. is a co-inventor on licensed patents held by the University of Goettingen. R.J.M, E.R.P., D.M.T., B.G. and J.E.H. are co-founders, scientific advisors and stockholders in Dynomics Incorporated. D.M.T. and B.G. are employees of Dynomics Inc. /Dynomics Pty Ltd. QIMR Berghofer Medical Research Institute has filed a patent on the use of BRD inhibitors.

AUTHOR CONTRIBUTIONS

R.J.M., S.J.H., G.A.Q-R., S.K., T.B., J.E.H., performed experiments, L.D., H.K.V.,L.R., E.M., developed cardiac organoid cultures, R.J.M., S.J.H., P.R.J.F., Q.A.Q-R., N.R.M., B.G., D.T., E.R.P., J.E.H., analysed data, R.J.M., S.J.H., M.J.S., C.R.E., K.P.A.MD., T.B., D.E.J, J.E.H, designed the project, R.J.M., S.J.H., M.J.S., C.R.E., K.P.A.MD., T.B., D.E.J, J.E.H, interpreted data, R.J.M., S.J.H., D.E.J, J.E.H wrote the manuscript, all authors edited the manuscript.